

01 Jun 2023

## Coating Condition Detection And Assessment On The Steel Girder Of A Bridge Through Hyperspectral Imaging

Pengfei Ma

Jiaoli Li

Ying Zhuo

Pu Jiao

*et. al.* For a complete list of authors, see [https://scholarsmine.mst.edu/civarc\\_enveng\\_facwork/2620](https://scholarsmine.mst.edu/civarc_enveng_facwork/2620)

Follow this and additional works at: [https://scholarsmine.mst.edu/civarc\\_enveng\\_facwork](https://scholarsmine.mst.edu/civarc_enveng_facwork)



Part of the [Structural Engineering Commons](#)

### Recommended Citation

P. Ma et al., "Coating Condition Detection And Assessment On The Steel Girder Of A Bridge Through Hyperspectral Imaging," *Coatings*, vol. 13, no. 6, article no. 1008, MDPI, Jun 2023.

The definitive version is available at <https://doi.org/10.3390/coatings13061008>





This work is licensed under a [Creative Commons Attribution 4.0 License](#).

This Article - Journal is brought to you for free and open access by Scholars' Mine. It has been accepted for inclusion in Civil, Architectural and Environmental Engineering Faculty Research & Creative Works by an authorized administrator of Scholars' Mine. This work is protected by U. S. Copyright Law. Unauthorized use including reproduction for redistribution requires the permission of the copyright holder. For more information, please contact [scholarsmine@mst.edu](mailto:scholarsmine@mst.edu).

## Article

# Coating Condition Detection and Assessment on the Steel Girder of a Bridge through Hyperspectral Imaging

Pengfei Ma <sup>1</sup>, Jiaoli Li <sup>1</sup>, Ying Zhuo <sup>1</sup>, Pu Jiao <sup>2</sup> and Genda Chen <sup>1,\*</sup>

<sup>1</sup> Department of Civil, Architectural, and Environmental Engineering, Missouri University of Science and Technology, Rolla, MO 65409, USA; pm7m8@mst.edu (P.M.); jlbtt@mst.edu (J.L.); yingzhuo@mst.edu (Y.Z.)

<sup>2</sup> Department of Computer Science, University of Kentucky, Lexington, KY 40506, USA; pujiao@uky.edu

\* Correspondence: gchen@mst.edu

**Abstract:** The organic coating of bridge steel girders is subjected to physical scratches, corrosion, and aging in natural weathering. The breakdown of the coating may cause serviceability and safety problems if left unnoticed. Conventional coating inspection is time-consuming and lacks information about the coating's chemical integrity. A hyperspectral imaging method is proposed to detect the condition of steel coatings based on coating-responsive features in reflectance spectra. A field test was conducted on the real-world bridge, which shows obvious signs of degradation. The hyperspectral signature enables an assessment of the coating's health and defect severity. The results indicated that the coating scratch can be effectively located in the domain of a hyperspectral image and the scratch depth can be determined by mapping a scratch depth indicator (SDI = R532 nm/R641 nm). Rust sources and products in steel girders can be identified by the unique spectral signatures in the VNIR range, and the rust stains (and thus stain areas) scattered on the coating can be pinpointed at pixel level by the chloride rust (CR) indicators >1.11 (CR = R733 nm/R841 nm). The chemical integrity of a topcoat is demonstrated by the short-wave infrared spectroscopy and the topcoat degradation can be evaluated by the decreased absorption at 8000 cm<sup>-1</sup> and 5850 cm<sup>-1</sup>. Hyperspectral imaging enables faster and more reliable coating condition detection by the spectral features and provides an alternative for multi-object coating detection.



**Citation:** Ma, P.; Li, J.; Zhuo, Y.; Jiao, P.; Chen, G. Coating Condition Detection and Assessment on the Steel Girder of a Bridge through Hyperspectral Imaging. *Coatings* **2023**, *13*, 1008. <https://doi.org/10.3390/coatings13061008>

Academic Editors: Qunfeng Zeng and Edoardo Proverbio

Received: 1 May 2023

Revised: 19 May 2023

Accepted: 24 May 2023

Published: 29 May 2023



**Copyright:** © 2023 by the authors. Licensee MDPI, Basel, Switzerland. This article is an open access article distributed under the terms and conditions of the Creative Commons Attribution (CC BY) license (<https://creativecommons.org/licenses/by/4.0/>).

**Keywords:** steel girder; nondestructive inspection; corrosion; coating degradation; spectroscopic analysis; hyperspectral imaging

## 1. Introduction

Steel has been a candidate in civil engineering, especially bridges, because of its high strength and light weight. There are many uses of steel components in suspension, cable-stay, and girder bridges to overcome the self-weight problem [1,2]. It can also be used as a superstructure for arch bridges to facilitate the construction of the deck and carry loads. For example, the Sydney Harbor Bay bridge [3]. In addition, steel is also widely used for girders in highway bridge networks (>30%) to provide more clearance for traffic [4]. However, steel components that are exposed to the natural weathering environment will be severely impaired by corrosive media, thus introducing safety and serviceability issues [4,5]. According to the Federal Highway Administration (FHWA) [6], statistics show that around 45% of steel bridges are structurally deficient, with 19% being almost structurally obsolete. Corrosion is currently the biggest concern for the structural integrity of steel components because corrosion can significantly (almost 40%) reduce fatigue strength [7–9]. For example, corrosion is illustrated as the reason for the sudden collapse of the I-35W steel deck truss bridge in Minneapolis, USA [10]. The deteriorated coating increased the chances of corrosion on the steel substrate [4]. Therefore, regular inspection is necessitated for coating, and its conditions should be assessed to ensure acceptable serviceability and protect the substrate from direct contact with corrosive factors [9].

Coatings are required to have protection against various degradations, whether physical or chemical [11]. The coating should be able to withstand physical impairments such as scratches and abrasions, as well as some aggressive species such as chlorides, acids, and water [4,11–13]. Coating defects are thus different depending on degradation exposures [13]. Many aspects of the coatings can be monitored to assess their condition, such as delamination, chalking, checking, and rust staining [13,14]. Visual inspection has long been practiced for bridge coating due to its reliable inspection quality. However, this method requires experienced practitioners, and the evaluation of coating condition assessment might be subjected to objective and quantifiable issues. Visual inspection is also time-consuming and labor-intensive, which makes it impossible in terms of regular inspection [15]. The electrochemical impedance spectroscopy (EIS) technique has been studied to detect coating integrity as well as substrate corrosion occurrence. Impedance values can effectively reflect the coating status before the presence of macroscopic degradations, but EIS does not give local information and thus a vague location of the impaired coating spots [16,17]. Spectroscopic techniques, including Fourier transform infrared spectroscopy (FTIR), Raman spectroscopy, and Mossbauer spectroscopy, have been performed to evaluate the coating conditions but are generally limited to lab experiments [11,18–20]. The image-based method has been implemented together with machine learning techniques over the last two decades to achieve fast inspection [21,22]. The pixel-level imagery features in conjunction with the artificial intelligence (AI) algorithm significantly improved efficiency and reliability, which might be a substitute for human inspection [21,23]. However, an apparent drawback is that red, green, and blue (RGB) images are unable to provide information about the coating chemicals, thus preventing a thorough assessment before the occurrence of the obvious defects [24]. In addition, it may confront some confusion in the detection if the defects are dominantly featured by color and the computer vision method is sensitive to the nonuniform illuminations on the detected surfaces [21].

Hyperspectral imaging (HSI) is emerging as a compromised tool for simultaneous spatial and spectral inspection because hyperspectral imaging possesses the RGB information and the surface composition information according to the response at different wavelengths [8,25]. Therefore, both spatial dysconnectivity and compositional inhomogeneity can be plotted in the context of hyperspectral imaging [25]. The technique has been utilized to quantitatively assess the coating thickness of the paint on the steel according to the spectral signature as well as the discrimination of different chemical binders and polymers in the coating composition for automatic coating condition detection [26–28]. Likewise, near-infrared (NIR) spectroscopy was used to evaluate the conversion of white pigment of the acrylate coatings exposed to ultraviolet (UV) radiation [28]. Hyperspectral imaging has also been tested to identify pinholes in the coating by introducing a matching filter at the pixel level [24]. To differentiate the colors from different objects in the girder coatings, Dayakar established a support vector machine (SVM) model, and the color yellow from corrosion rust in different environments, acid or sulfate, can be discriminated against with 94% accuracy [3]. Hyperspectral imaging was also practiced in an arch bridge truss coating assessment. The proposed multi-class SVM can generate highly accurate coating assessment results by integrating information from only 21 bands in the range of the visible spectrum [29]. However, the application of hyperspectral imaging is mainly focused on the characterization of coating degradation in the lab. It is noted that the established method based on HSI for coating defect identification and condition assessment in real structures is not sufficient.

In this study, hyperspectral imaging is proposed to inspect the coatings on the steel girder of a real bridge. Some typical coating defects under natural weathering exposures are preselected for hyperspectral scanning to demonstrate their capability. The hyperspectral results are validated with ground-truth lab characterizations, FTIR, scanning electron microscope (SEM), and energy-dispersive X-ray spectroscopy (EDS), to illustrate the applicability of hyperspectral imaging techniques in coating condition detection and assessment. It is found that the coating scratch profiles can be detected, and the scratch depth is character-

ized by the spectral signatures of the coating layers and substrate. The chemically degraded coating can be distinguished from the sound coating by hyperspectral reflectance features in short-wave infrared (SWIR). In addition, the rust stains can be identified without color bias by hyperspectral imaging, and the rust medium can be recognized according to the unique spectral signatures of rust products.

## 2. Materials and Methods

The proposed hyperspectral imaging technique for coating condition detection is demonstrated on a continuous girder bridge on the main road of 10th Street (37.951454, −91.769034), Rolla, Missouri, USA. The bridge is an eight-span steel girder bridge with a span configuration of 15.79 m, 15.54 m, 16.46 m, 18.59 m, 18.89 m, 12.49 m, 16.15 m, and 11.85 m (totaling 125.5 m) from west to east as shown in Figure 1. The steel used in the bridge girder is fabricated structural carbon with a nominal yield strength of 20,000 psi. W30 and W33 steel girders were used for the continuous-span bridge to provide more clearance for the railway.

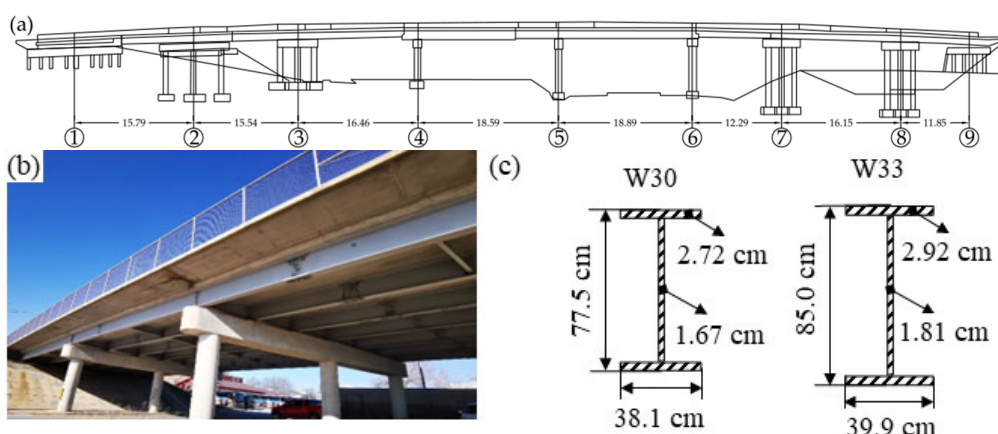


**Figure 1.** (a) the original drawing of the bridge design; (b) a view of the real test bridge; (c) steel girder dimension.

The bridge was constructed in 1974, and the steel girders were originally coated with brown lead silicochromate. The coating was removed in 2002 due to health concerns in terms of lead and was replaced by the current calcium sulfonate pigmented alkyd coating coupled with epoxy primer, as shown in Figure 2. Calcium sulfonate alkyd paint is designed for replacement due to its significant corrosion-inhibition effect. The substitution of calcium sulfonate alkyd is due to its continuous release of corrosion inhibitors. Moreover, the multilayer coating system can significantly prevent the ingress of corrosive ions due to the more compact interface between alkyd and epoxy, as demonstrated by the scanning Kelvin probe (SKP) [30]. This bridge was selected as the research object because of the presence of various typical coating defects on the girders. In addition, an alkyd topcoat is also one of the most widely used paints in current bridge protection [4].

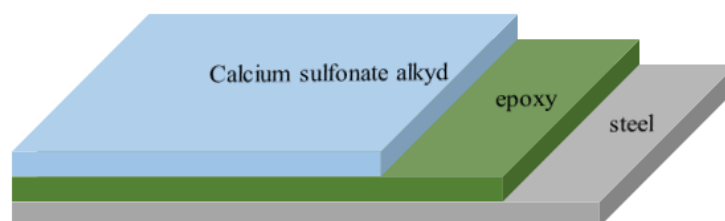


**Figure 2.** Coating system demonstration for the steel girder.

To characterize the coating defects with hyperspectral imaging, the preselected spots of interest (SOI) on the girder coating were scanned with a Headwall dual-lens hyperspectral

(Headwall phonetic, Boston, MA, USA) camera as shown in Figure 3. The camera has a 1.2 m standoff from the SOIs. Under natural light radiation, the exposure time was set to 45 ms accordingly to prevent overexposure in the hyperspectral image. The hyperspectral camera in this study enables the spectral range of visible and near-infrared (VNIR, 400–1000 nm) and short-wave infrared (SWIR, 1000–2500 nm) with a spectral resolution of 2.21 nm in VNIR and 6.02 nm in SWIR. Prior to every HSI collection, the dark was captured with the cap on to reduce the internal current noise in the image. Likewise, white reference was also collected for the conversion of the raw digital numbers to radiance and finally reflectance. In this test, the camera was supported by a tripod because the SOIs are accessible; otherwise, the camera can be integrated into an unmanned aerial vehicle for coating inspection.

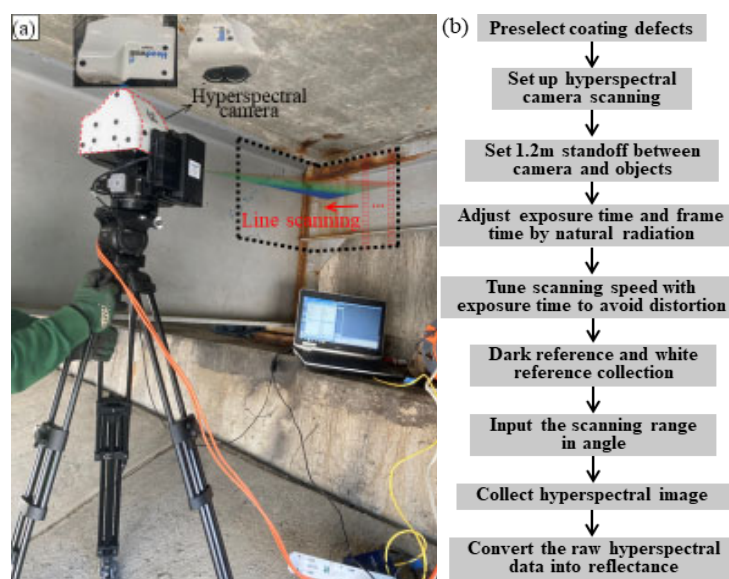


**Figure 3.** (a) Setup for hyperspectral imaging collection in the field; (b) data collection configuration.

Hyperspectral imaging is indeed a subset of the spectroscopic technique for polymer characterization in this study. As the hyperspectral imaging in this study enables wavenumbers from  $4000\text{ cm}^{-1}$  to  $10,000\text{ cm}^{-1}$ , it is characterized by band combinations, coupling, and overtones [28]. Therefore, FTIR is used to validate the hyperspectral results. Some coating samples are retrieved from the bridge for analysis. The FTIR spectra were recorded with a Nicolet™ iS50 FTIR Spectrometer (Thermo Fisher Scientific, Waltham, MA, USA) in the spectral range between  $400\text{ cm}^{-1}$  and  $4000\text{ cm}^{-1}$  with a resolution of  $4\text{ cm}^{-1}$ . For each sample, 16 runs were performed to enhance the spectra and reduce the noise. The FTIR spectra are presented in transmittance for easy comparison in this study. In addition, scanning electron microscopy (SEM) was performed on coating (rust-stained, healthy, and degraded) samples using a Helios Hydra CX (Thermo Fisher Scientific, Waltham, MA, USA) with an accelerating voltage of 15 kV and a beam current of 0.8 nA under high vacuum pressure ( $<5.0 \times 10^{-4}\text{ Pa}$ ). The working distance between the lens and the sample was set to 4 mm. To determine the atomic distribution on the topcoat, EDS energy-dispersive X-ray spectroscopy (EDS) was performed with a Thermo Noran Ultra Dry 60 mm<sup>2</sup> detector (Thermo Fisher Scientific, Waltham, MA, USA) by mapping in the Pathfinder X-ray Microanalysis Software-2022 (Thermo Fisher Scientific, Waltham, MA, USA). As the organic coating in this study is nonconductive, all samples were coated with a thin film of gold/palladium (Au/Pd) by sputtering for 45 s to prevent charging.

### 3. Results and Discussion

#### 3.1. Coating Scratch

Figure 4 presents a view of the coating scratch on the bridge steel girder. It is observed that the scratch depth varies along the trace as the scratch even reaches the undercoat in

some areas. The coating thickness is reduced, though the color difference from the original view is not significant. In addition, it is not known whether the substrate steel is exposed due to scratches. A coating is used to protect the steel from corrosive media. Corrosion can initiate at a bare steel spot, and the effect gradually propagates concentrically to the local area, which progressively damages the health coatings. Figure 4b shows the comparison of the spectral signatures in the range of 400–1000 nm (visible and near-infrared, VNIR) from different objects, topcoat (pigmented alkyd), undercoat (epoxy), and girder steel, in the domain of scratches from the hyperspectral imaging. In view of hyperspectral imaging, those three objects are spectrally different, especially for the topcoat and undercoat, though both are organic polymers that are characterized by aromatic rings and side chains. As for the substrate, steel does not yield any absorption features in the range of VNIR because it is composed of metal ions, which do not absorb photons in the current wavelength domain [29].

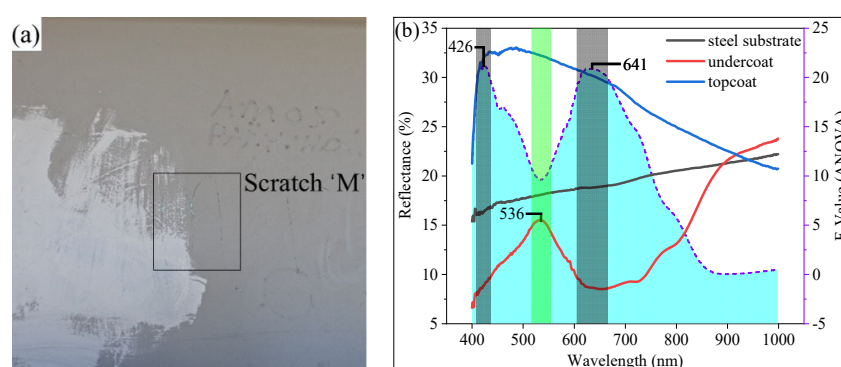


**Figure 4.** Coating scratch on the steel girder. (a) Original view; (b) spectral signatures of different coating layers and the corresponding F-values from ANOVA analysis of spectra.

To differentiate different layers of coating, a scratch depth indicator (SDI) is developed by comparing the ratio between two bands, 536 nm and 641 nm. Figure 4b displays the F-value results derived from the one-way ANOVA analysis based on the spectra from the three objects. There are two local maxima at 426 nm and 641 nm and one local minimum at 536 nm. According to the ANOVA F-value, spectra at wavelength 536 nm yield the least variation ( $p < 0.05$ ) in the range of 400–750 nm. For comparison, 426 nm and 641 nm are more sensitive to the differences between different coating layers because higher close F-values are observed, which are around 21 ( $p < 0.05$ ). To establish a robust indicator, 641 nm is selected as the most sensitive band in this study because 426 nm is located at the beginning of the spectrum, which is usually subjected to severe mechanical noises [8]. Figure 5a demonstrates the mapping of SDI (536 nm/641 nm) in hyperspectral imaging. The scratch profile can be easily identified, and the exposed undercoat can be located by the black spots. For the RGB method, the color feature of the scratch is used to identify the scratch profile, and the result is easily subjected to false detection if objects with similar colors are present [31]. In order to assess the scratch condition, different layers of the coating are retrieved from the mapping by thresholds to demonstrate the scratch depth. The corresponding SDI threshold for undercoat and steel is obtained from the distribution of the SDI values, as illustrated in Figure 5c,f. For undercoat epoxy, the critical SDI of 1.33 isolates the exposed undercoat, though some scattered misidentifications can be observed. Most of the misclassifications of the undercoat are located in the shades of the white reference board. This is because the shade can distort the spectra and thus produce incorrect information, which can be eliminated by the additional external light source in real practice [26]. It is noted that several pixels are distinguished from the undercoat in the heart of scratch “M”, which is the substrate steel. As hyperspectral imaging also enables a high spatial resolution of 0.56 mm in this study, the exposed steel can be spotted by the critical SDI of 0.95. The selection of the critical SDI in this study is because 95% of the calculated SDI from the

pixels on the steel substrate are between 0.95 and 1.02. There are in total 5 pixels (pixel dimension:  $0.56 \times 0.56$  mm) that can be identified, which makes a  $1.57 \text{ mm}^2$  exposure. It is worth noting that hyperspectral imaging can perform a much more accurate inspection by using spectral information compared to RGB inspection because the resolution is not high enough to identify such small defects [21,22].

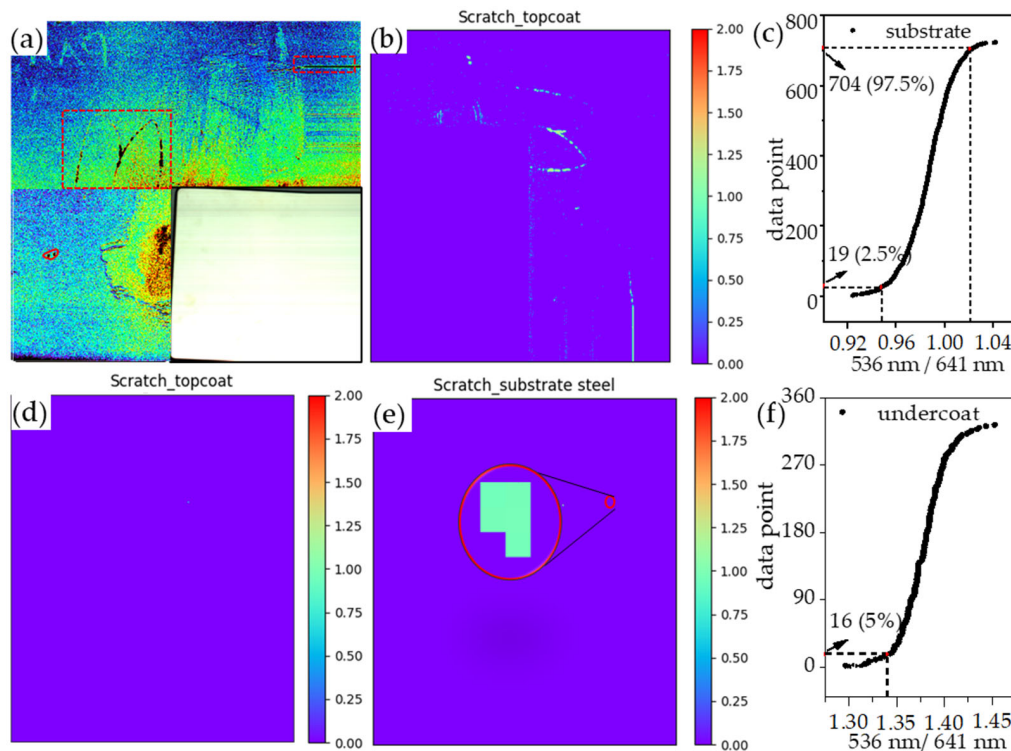


**Figure 5.** Different layers of the girder coating with scratches. (a) Mapping of SDI (536 nm/641 nm) in hyperspectral imaging; (b) scratch of undercoat (SDI > 1.33); (c) derivation of the critical SDI for undercoat; (d) topcoat; (e) scratch of substrate steel ( $0.95 < \text{SDI} < 1.02$ ); (f) derivation of the critical SDI for steel.

### 3.2. Steel Rust Stains

The steel rust percentage has been used as an indicator to assess the coating conditions according to ASTM D610-08 for timely remedies [23,31]. Figure 6 presents the coating surface with steel rust stains as well as the corroded steel girder top flange. Many corrosive media cause rust in the atmospheric environment, and the corrosion products may vary. Acidic exposures are prone to producing magnetite ( $\text{Fe}_3\text{O}_4$ ), ferrous chloride ( $\text{FeCl}_2$ ), and iron oxide-hydroxide ( $\text{FeOOH}$ ) [31]. For chloride salt ions attack, akageneite ( $\beta\text{-FeOOH}$ ) and goethite ( $\alpha\text{-FeOOH}$ ) are the main corrosion products [31,32]. Two steel plates treated with sodium chloride and water, respectively, are prepared and placed in the scanning view. Figure 6b shows the spectral signatures in the VNIR range derived from corrosion spots on two plates. It is noted that the rust products with different exposures differ spectrally. Rust obtained from sodium chloride solution yields three absorption features at 612 nm, 733 nm, and 841 nm, and water-based corrosion products have features at 708 nm and 950 nm, which are characterized by water [8]. The spectra for the corrosion rust from different sources are consistent with the previous study [33].

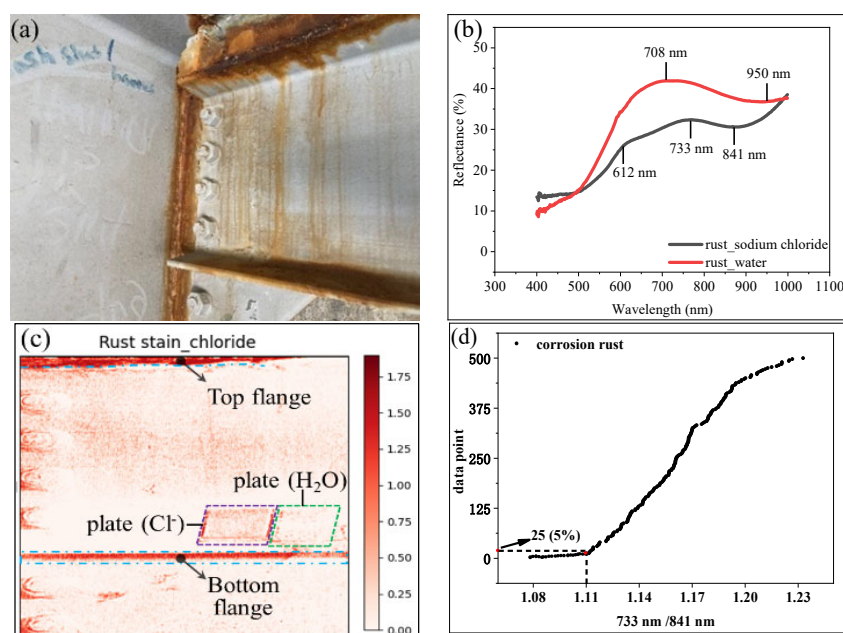


**Figure 6.** Girder coating with rust stain. (a) The view of the rust spot; (b) spectral signatures of the different rust products in VNIR; (c) rust stain demonstration by CR indicator ( $>1.11$ ); (d) critical CR for rust stain on topcoat.

As chloride corrosion is more aggressive, it is worth emphasizing its corrosion effect before the pervasive attack on both substrate and organic coatings [14]. The chloride rust (CR) indicator, 733 nm/841 nm, is constructed to demonstrate the corrosion products. Figure 6c demonstrates the mapping of CR in the domain of hyperspectral imaging with a threshold of 1.11. This critical CR is obtained from the stain pixels in the diaphragm with the same method as illustrated in SDI. The severely rusted steel flanges can be identified in CR mapping as indicated by the dark red areas. Moreover, the rust stain on the coating in the diaphragm is also detected by the CR, though the CR values are smaller compared to the rust spots. It is because rust products intermingle with the topcoat in the domain of a pixel. The hyperspectral spectrum is representative of the overall composition of the chemicals in that pixel [8]. As for the rust spot inspection, the hyperspectral imaging technique greatly reduced the false detection as opposed to the RGB method [33].

The coating samples with rust stains are analyzed by energy-dispersive X-ray spectroscopy (EDS) as opposed to the normal coating on this girder. Figure 7 shows the comparison of the element mapping results. The EDS spectrum as shown in Figure 7a demonstrates detectable peaks in terms of chloride (Cl) for the rust-stained coating, while the rust-free coating is dominated by the topcoat polymer compositional elements, carbon (C) and oxygen (O). The presence of Cl is also reflected by the element mapping result, as illustrated in Figure 7b. For elements related to steel rust, Fe and Cl show significant differences in distribution. Oxygen (O) is not considered here to distinguish rust because of its massive existence in alkyd resins and thus cannot be easily impacted [34]. As seen from Figure 7b, Fe is more visible on the coating with rust stains, though Fe is also spotted in the rust-free coating samples. For Cl, the contrast is more significant because it almost disappears in rust-free samples. Table 1 shows the element ratio of each detectable element present on the coating surface. C and O occupy, in total, about 90% of the coating topology, and nitrogen (N) is the third prevailing element that makes up around 7.5% of the coating topology. The elemental dominance agrees well with the composition of alkyd. The rust-stained coating has Fe of 1.78%, which is higher than the 0.56% in the rust-free coating. As for Cl, it occupies 0.51% of the total detectable elements for the topcoat with rust stains in comparison with 0% Cl in the stain-free topcoat. Element Cl distinguishes the rust-contaminated coatings from the rust-free sample, which shows negligible presence.



The result is consistent with the hyperspectral imaging result, which shows the rust stain distribution as well as the corrosion source as Cl-related media.

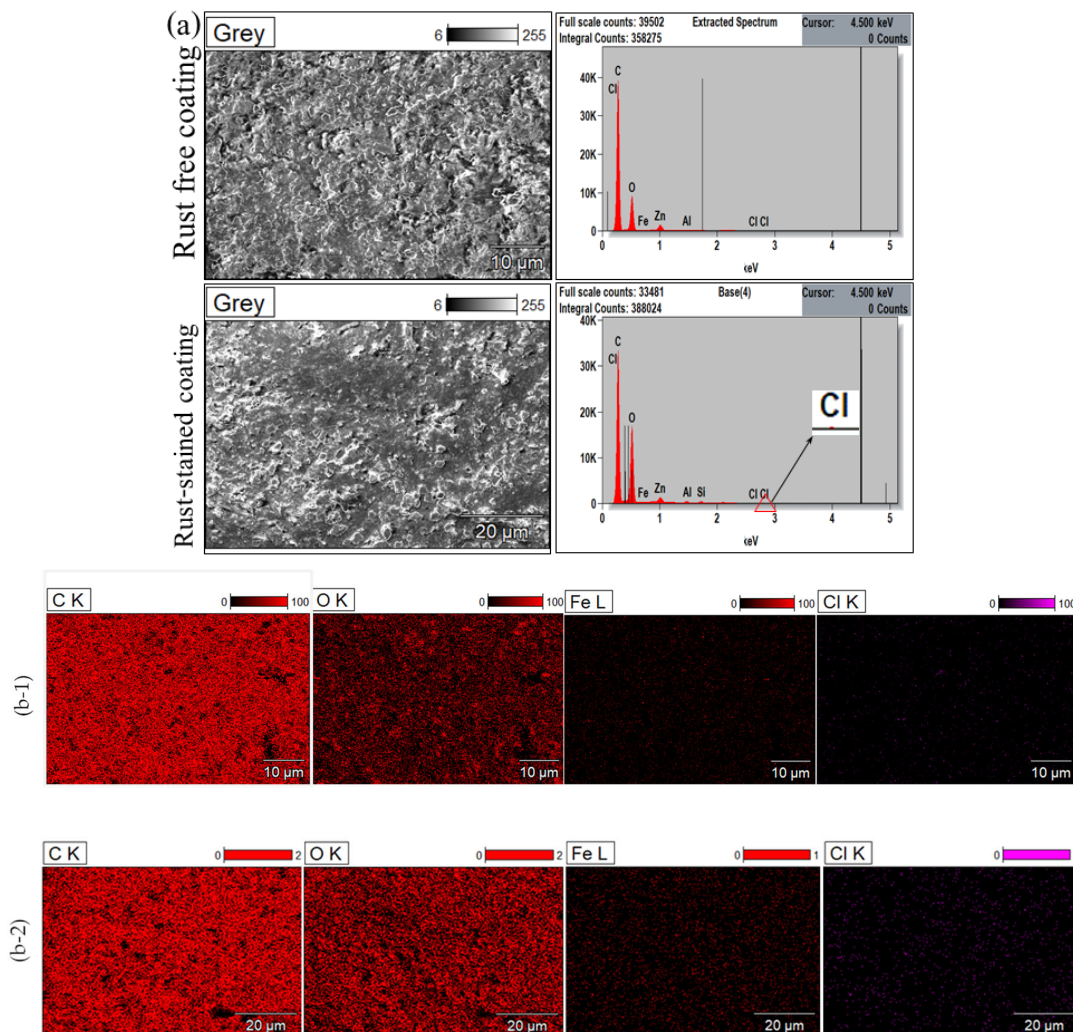


**Figure 7.** Comparison of the element distribution on the coating with and without rust stains by (a) EDS spectra, (b-1) element distribution of rust-free topcoat from EDS mapping, (b-2) element distribution of rust-stained topcoat from EDS mapping.

**Table 1.** Percent of the detachable elements on the coating with and without rust stain.

Element	C	O	N	Fe	Cl	Al	Zn
Rust-free coating	54.34	36.00	7.31	0.56	0	0.48	1.31
Rust-stained coating	53.15	34.98	7.43	1.78	0.51	0.38	1.53

### 3.3. Degraded Topcoat

A degraded topcoat can expose the undercoat and thus increase the corrosion probability of the substrate. Early detection can potentially enhance the serviceability of steel girders. Figure 8 shows the deteriorated topcoat on the bottom flange of the steel girders in the proposed field bridge. Those deteriorated topcoats have lost their cling to the undercoat and thus cannot effectively protect the undercoat and substrate. As the degradation is generally characterized by chain breakage due to oxidation, Figure 9 displays the comparison between healthy and degraded topcoats by both FTIR and SWIR spectroscopy from hyperspectral imaging. FTIR provides complementary information for SWIR spectroscopy to interpret the topcoat degradation in view of the binder's chemical connections.

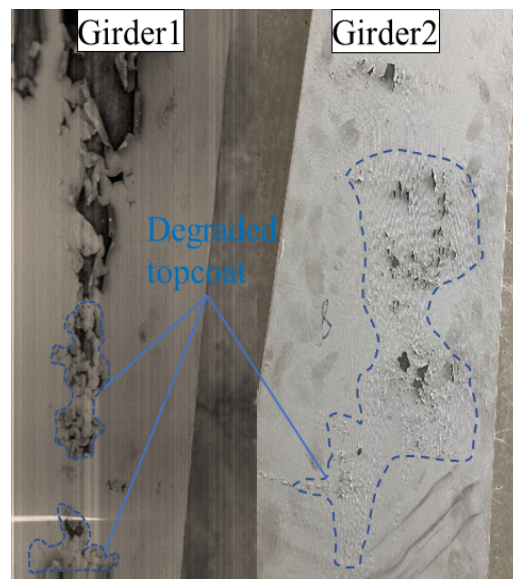


**Figure 8.** Demonstration of the degraded topcoat on the bottom flange of the steel girder.

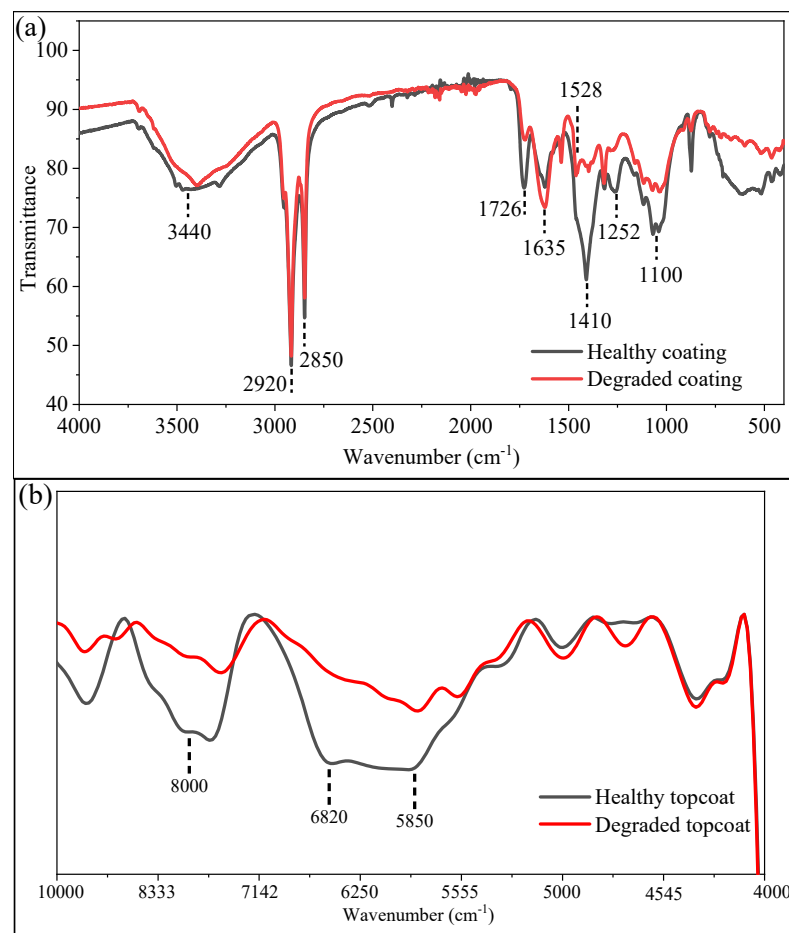


**Figure 9.** Comparison of the healthy and degraded topcoat in the range of (a) 400–4000  $\text{cm}^{-1}$  (FTIR), (b) 4000–10,000  $\text{cm}^{-1}$  (SWIR).

Considering the natural aging and atmospheric exposure effects on the topcoat, the stretching vibrations of the C=O at 1726  $\text{cm}^{-1}$  and C–O–C at 1528  $\text{cm}^{-1}$  are featured by the bond cleavage in the polyester of the girder topcoat, alkyd resin [35,36]. Table 2 sum-

marizes the band assignment of the alkyd resin. It can be seen that the narrow absorption bands at  $1726\text{ cm}^{-1}$  and  $1528\text{ cm}^{-1}$  both significantly decrease for the degraded topcoat in comparison to the healthy, which indicates the chains shortening in the polymer [36]. The chain scission in polyester is also observed by the decreasing absorption at  $2920\text{ cm}^{-1}$  and  $2850\text{ cm}^{-1}$  for degraded topcoat, which illustrates the reduced presence of the side chains [37]. In addition, the O–C–O featured band at  $1410\text{ cm}^{-1}$  almost disappears to demonstrate the reduction side chain [38]. On the contrary, it is noted that  $1635\text{ cm}^{-1}$  is boosted due to the degradation effect on the topcoat [36,39]. It is because of the autoxidation of the polymer crosslink. In this process, the degraded alkyd resin releases alcohol and carbonyl species, which thus reduces the molecular weight of the original topcoat component [37]. The decreasing weight of alkyd resin can also be implied by the diminished bands at  $1100\text{ cm}^{-1}$  and  $1252\text{ cm}^{-1}$ . The breakage of C–O–C produces volatile species, for example, phthalic acid due to the Norrish Type I reaction [39]. Figure 10 shows the microstructure of the healthy and deteriorated topcoats by SEM. In comparison, the degraded topcoat yields a messier topology, and the topcoat has been degraded into more pieces. Table 3 illustrates the presence of detectable elements on the topcoat derived from the EDS mapping results. C is significantly reduced from the healthy to the degraded topcoat due to the oxidation effect, which conforms to the FTIR results.

**Table 2.** Major bands of alkyd resin in FTIR and its band assignment.

Wavenumber ( $\text{cm}^{-1}$ )	Assignment
741–705	Aromatic out-of-plane bending
<1000	Ring vibrations and C–X (with X=Cl or $\text{CH}_3$ ) coupling
1070	Aromatic in-plane bending
1119	C–O–C stretching
1258	C–O–C stretching
1340–1300	Vibrations involving the aromatic rings
1429	O–C–O bending
1528	C–O–C bending
1590	Aromatic in-plane bending
1650–1500	C=N, C=O
1635	C=C stretching
1726	C=O stretching vibration carboxylic acids and esters
2850	(C–H)- $\text{CH}_2$ symmetric stretching
2921	(C–H)- $\text{CH}_2$ asymmetric stretching
3440/3314	OH stretching

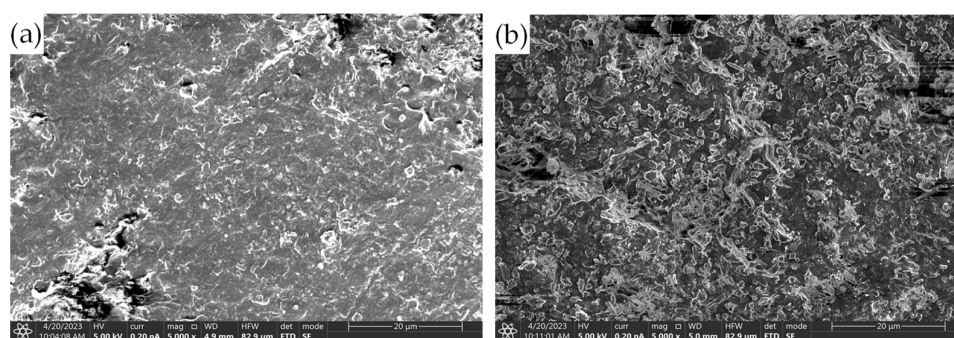


**Figure 10.** Topology by SEM of (a) healthy topcoat; (b) degraded topcoat.

**Table 3.** Percentage of the detachable elements on the coating with and without rust stains.

Element	C	O	N	Fe	Cl	Al	Zn
Healthy topcoat	53.15	37.53	7.43	0.43	0	0.52	1.37
Degraded topcoat	42.19	48.47	7.58	0.25	0	0	1.50

Figure 9b presents the spectra derived from the healthy and the degraded topcoat in the range of 4000–10,000  $\text{cm}^{-1}$  after continuum removal processing to facilitate quantitative comparison [28,39]. As illustrated in the FTIR, the main and side chains were greatly shortened due to the degradation effect. The reduction of the C=O in the degraded topcoat can also be detected in SWIR spectroscopy by the carbonyl stretching characterized bands at 5850  $\text{cm}^{-1}$  [40]. This band should be the overtones of the fundamental vibration of the carbonyl groups illustrated in 400–2000  $\text{cm}^{-1}$ . A similar decreasing trend at 5850  $\text{cm}^{-1}$  is also observed on the alkyd resins under ultra-violet exposure [41]. Another significant difference is located around 6820  $\text{cm}^{-1}$ , characterized by the second overtone of the hydroxyl group [8,41]. The absorption feature is almost gone due to the deterioration of the topcoat. The deletion of hydroxyl groups is also observed by the absorption at 3440  $\text{cm}^{-1}$  [36,37]. However, band 3440  $\text{cm}^{-1}$  remains significant, though it has decreased. It is because 3440 is characterized by not only the bending vibration of hydroxyl but also water [8]. The third recognizable spectral zone that differentiates healthy and degraded topcoats is around 8000  $\text{cm}^{-1}$ . This absorption intensity of this broadband shrinks due to the degradation of the topcoat, which is attributed to the loss of the oxygenated products, singly doubly bonded oxygen, due to photooxidation [40].

#### 4. Conclusions

The manuscript presents a study that uses hyperspectral imaging to detect coating defects in bridge steel girders. Coating scratch, substrate rust, and topcoat degradation are evaluated. The major findings can be summarized as follows:

- i. Scratch profiles can be effectively depicted by scratch depth indicators by applying a critical threshold for each coating layer. The epoxy undercoat can be discriminated against by  $\text{SDI} > 1.33$ , and the exposed substrate is identified by  $0.95 < \text{SDI} < 1.02$ .
- ii. The source of the corrosion products can be evaluated by the absorption features at 612, 708, 733, 841, and 950 nm in the VNIR range. Water-based corrosion products yield features at 708 and 950 nm, while chloride-based rust features absorption at 612, 733, and 841 nm.
- iii. The rust-stained coating can be estimated by the corrosion rust indicators ( $\text{CR} (\text{R733}/\text{R841}) > 1.11$ ), and the total area of the corrosion spot can then be calculated by the pixel dimensions.
- iv. As for the degraded topcoat, SWIR spectra show significant reduction at 8000  $\text{cm}^{-1}$ , 5850  $\text{cm}^{-1}$  as well as hydroxyl absorption at 6820  $\text{cm}^{-1}$ .

For a more robust inspection of the girder coatings, further work should focus on the quantitative study of how the SWIR spectra can evaluate the severity of the coating degradations. And more types of industrial coatings need to be tested with hyperspectral imaging to determine the corresponding indicator to differentiate their presence from other layers, which can greatly expand the application of hyperspectral imaging in fast nondestructive inspection of the girder coating conditions.

**Author Contributions:** Conceptualization, methodology, investigation, writing original draft preparation, P.M.; methodology, investigation, J.L.; methodology, Y.Z. and P.J.; review and funding acquisition, G.C. All authors have read and agreed to the published version of the manuscript.

**Funding:** Financial support to complete this study was provided by the US Department of Transportation, Office of the Assistant Secretary for Research and Technology (USDOT/OST-R) under Grant No. 69A3551747126 through the INSPIRE University Transportation Center (<https://inspire-utc.mst.edu>, accessed on 23 May 2023) at Missouri University of Science and Technology. The views, findings, and conclusions reflected in this publication are solely those of the authors and do not represent the official policy or position of the USDOT/OST-R, or any state or other entity.

**Institutional Review Board Statement:** Not applicable.

**Informed Consent Statement:** Not applicable.

**Data Availability Statement:** Not applicable.

**Acknowledgments:** The authors wish to thank Ibrahim Alomari and Peter Ogunjinmi for their assistance during hyperspectral data collection at the bridge site.

**Conflicts of Interest:** The authors declare no conflict of interest.

## References

1. Kitada, T. Considerations on recent trends in, and prospects of, steel bridge construction in Japan. *J. Constr. Steel Res.* **2006**, *62*, 1192–1198. [CrossRef]
2. Ma, P.; An, J.; Zhang, B.; Zhu, P.; Zhao, H. Research on Axle Load Recognition Algorithm Based on U-rib Transverse Influence Line. *Highw. Eng.* **2020**, *45*, 9. [CrossRef]
3. Mustapha, S.; Huynh, C.P.; Runcie, P.; Porikli, F. Paint condition assessment of civil structures using hyper-spectral imaging. In Proceedings of the 7th International Conference on Structural Health Monitoring of Intelligence Infrastructure—SHMII 2015, Torino, Italy, 1–3 July 2015; Intl Society for Structural Health Monitoring of Intelligent Infrastructure: Red Hook, NY, USA, 2015.
4. Yanez, L.M.M. Bridge Maintenance to Enhance Corrosion Resistance and Performance of Steel Girder Bridges. Ph.D. Thesis, Purdue University, West Lafayette, IN, USA, 2016.
5. Zhang, L.; Lv, X.; Lau, K.; Viswanathan, S.; Li, M.; Gosain, P. *Assessment of Structural Steel Coating Applications*; Florida Department of Transportation: Tallahassee, FL, USA, 2021.
6. FHWA; USDOT. *Bridges and Structures—Bridges by Year Built 2013*; Federal Highway Administration; US. Department of Transportation: Washington, DC, USA, 2015. Available online: <http://www.fhwa.dot.gov/bridge/structyr.cfm> (accessed on 20 April 2023).
7. Menga, A.; Kanstad, T.; Cantero, D.; Bathen, L.; Hornbostel, K.; Klausen, A. Corrosion-induced damage and failures of posttensioned bridges: A literature review. *Struct. Concr.* **2023**, *24*, 84–99. [CrossRef]
8. Ma, P.; Fan, L.; Chen, G. Hyperspectral reflectance for determination of steel rebar corrosion and Cl<sup>-</sup> concentration. *Constr. Build. Mater.* **2023**, *368*, 130506. [CrossRef]
9. Lazorenko, G.; Kasprzhitskii, A.; Nazdracheva, T. Anti-corrosion coatings for protection of steel railway structures exposed to atmospheric environments: A review. *Constr. Build. Mater.* **2021**, *288*, 123115. [CrossRef]
10. Guo, S.; Si, R.; Dai, Q.; You, Z.; Ma, Y.; Wang, J. A critical review of corrosion development and rust removal techniques on the structural/environmental performance of corroded steel bridges. *J. Clean. Prod.* **2019**, *233*, 126–146. [CrossRef]
11. Cook, D.C. Spectroscopic identification of protective and non-protective corrosion coatings on steel structures in marine environments. *Corros. Sci.* **2005**, *47*, 2550–2570. [CrossRef]
12. Chong, S.L. A Comparison of Accelerated Tests for Steel Bridge Coatings in Marine Environments. *J. Prot. Coat. Linings* **1997**, *14*, 20. Available online: <http://worldcat.org/issn/87551985> (accessed on 27 May 2023).
13. Liao, K.W.; Lee, Y.T. Detection of rust defects on steel bridge coatings via digital image recognition. *Autom. Constr.* **2016**, *71*, 294–306. [CrossRef]
14. Corrosionpedia. Coating Failures and Defects. 2016. Available online: <https://www.ppcoatings.co.uk/wp-content/uploads/2016/06/Coating-Failure-Defects.pdf> (accessed on 23 May 2023).
15. Yao, Y.; Kodumuri, P.; Lee, S.K. *Performance Evaluation of One-Coat Systems for New Steel Bridges*; No. FHWA-HRT-11-046; United States Department of Transportation; Federal Highway Administration: Washington, DC, USA, 2011.
16. Waters, N.; Connolly, R.; Brown, D.; Laskowski, B. Electrochemical impedance spectroscopy for coating evaluation using a micro sensor. In Proceedings of the Annual Conference of the PHM Society, Fort Worth, TX, USA, 29 September–2 October 2014; Volume 6. [CrossRef]
17. Hayashibara, H.; Tada, E.; Nishikata, A. Monitoring the early stage of degradation of epoxy-coated steel for ballast tank by electrochemical impedance spectroscopy. *Mater. Trans.* **2017**, *58*, 1687–1694. [CrossRef]
18. Kanbayashi, T.; Ishikawa, A.; Matsunaga, M.; Kobayashi, M.; Kataoka, Y. Application of confocal raman microscopy for the analysis of the distribution of wood preservative coatings. *Coatings* **2019**, *9*, 621. [CrossRef]
19. Müller, J.; Knop, K.; Thies, J.; Uerpmann, C.; Kleinebudde, P. Feasibility of Raman spectroscopy as PAT tool in active coating. *Drug Dev. Ind. Pharm.* **2010**, *36*, 234–243. [CrossRef]
20. Hayes, P.A.; Vahur, S.; Leito, I. ATR-FTIR spectroscopy and quantitative multivariate analysis of paints and coating materials. *Spectrochim. Acta Part A Mol. Biomol. Spectrosc.* **2014**, *133*, 207–213. [CrossRef] [PubMed]
21. Potenza, F.; Rinaldi, C.; Ottaviano, E.; Gattulli, V. A robotics and computer-aided procedure for defect evaluation in bridge inspection. *J. Civ. Struct. Health Monit.* **2020**, *10*, 471–484. [CrossRef]
22. Feroz, S.; Abu Dabous, S. UAV-Based Remote Sensing Applications for Bridge Condition Assessment. *Remote Sens.* **2021**, *13*, 1809. [CrossRef]
23. Li, Y.; Kotsos, A.; Bartoli, I. Automated rust-defect detection of a steel bridge using aerial multispectral imagery. *J. Infrastruct. Syst.* **2019**, *25*, 04019014. [CrossRef]
24. Chen, M.; Lu, G.; Wang, G. Discrimination of Steel Coatings with Different Degradation Levels by Near-Infrared (NIR) Spectroscopy and Deep Learning. *Coatings* **2022**, *12*, 1721. [CrossRef]
25. Garrett, J.L.; Johansen, T.A.; Orlandić, M.; Bashir, M.A.; Raeissi, B. Detecting Pinholes in Coatings with Hyperspectral Imaging. In Proceedings of the 2021 11th Workshop on Hyperspectral Imaging and Signal Processing: Evolution in Remote Sensing (WHISPERS), Amsterdam, The Netherlands, 24–26 March 2021; IEEE: New York, NY, USA, 2021; pp. 1–5. [CrossRef]

26. Sandak, J.; Sandak, A.; Legan, L.; Retko, K.; Kavčič, M.; Kosel, J.; Poohphajai, F.; Diaz, R.H.; Ponnuchamy, V.; Sajinčič, N.; et al. Nondestructive evaluation of heritage object coatings with four hyperspectral imaging systems. *Coatings* **2021**, *11*, 244. [[CrossRef](#)]
27. Dingemans, L.M.; Papadakis, V.M.; Liu, P.; Adam, A.J.; Groves, R.M. Quantitative coating thickness determination using a coefficient-independent hyperspectral scattering model. *J. Eur. Opt. Soc.-Rapid Publ.* **2017**, *13*, 40. [[CrossRef](#)]
28. Daikos, O.; Heymann, K.; Scherzer, T. Monitoring of thickness and conversion of thick pigmented UV-cured coatings by NIR hyperspectral imaging. *Prog. Org. Coat.* **2018**, *125*, 8–14. [[CrossRef](#)]
29. Huynh, C.P.; Mustapha, S.; Runcie, P.; Porikli, F. Multi-class support vector machines for paint condition assessment on the Sydney Harbour Bridge using hyperspectral imaging. *Struct. Monit. Maint.* **2015**, *2*, 181–197. [[CrossRef](#)]
30. Doherty, M.; Sykes, J.M. Micro-cells beneath organic lacquers: A study using scanning Kelvin probe and scanning acoustic microscopy. *Corros. Sci.* **2004**, *46*, 1265–1289. [[CrossRef](#)]
31. Lavadiya, D.N.; Sajid, H.U.; Yellavajjala, R.K.; Sun, X. Hyperspectral imaging for the elimination of visual ambiguity in corrosion detection and identification of corrosion sources. *Struct. Health Monit.* **2022**, *21*, 1678–1693. [[CrossRef](#)]
32. Greenler, R.G. Infrared study of adsorbed molecules on metal surfaces by reflection techniques. *J. Chem. Phys.* **1966**, *44*, 310–315. [[CrossRef](#)]
33. De Kerf, T.; Pipintakos, G.; Zahiri, Z.; Vanlanduit, S.; Scheunders, P. Identification of corrosion minerals using shortwave infrared hyperspectral imaging. *Sensors* **2022**, *22*, 407. [[CrossRef](#)]
34. Kızılkonca, E.; Erim, F.B. Development of anti-aging and anticorrosive nanoceria dispersed alkyd coating for decorative and industrial purposes. *Coatings* **2019**, *9*, 610. [[CrossRef](#)]
35. Anghelone, M.; Stoytschew, V.; Jembrih-Simbürger, D.; Schreiner, M. Spectroscopic methods for the identification and photostability study of red synthetic organic pigments in alkyd and acrylic paints. *Microchem. J.* **2018**, *139*, 155–163. [[CrossRef](#)]
36. Anghelone, M.; Jembrih-Simbürger, D.; Schreiner, M. Influence of phthalocyanine pigments on the photo-degradation of alkyd artists' paints under different conditions of artificial solar radiation. *Polym. Degrad. Stab.* **2016**, *134*, 157–168. [[CrossRef](#)]
37. Duce, C.; Della Porta, V.; Tiné, M.R.; Spepi, A.; Ghezzi, L.; Colombini, M.P.; Bramanti, E. FTIR study of ageing of fast drying oil colour (FDOC) alkyd paint replicas. *Spectrochim. Acta Part A Mol. Biomol. Spectrosc.* **2014**, *130*, 214–221. [[CrossRef](#)]
38. Christensen, P.A.; Dilks, A.; Egerton, T.A.; Lawson, E.J.; Temperley, J. Photocatalytic oxidation of alkyd paint films measured by FTIR analysis of UV generated carbon dioxide. *J. Mater. Sci.* **2002**, *37*, 4901–4909. [[CrossRef](#)]
39. Zahiri, Z.; Laefer, D.F.; Gowen, A. The feasibility of short-wave infrared spectrometry in assessing water-to-cement ratio and density of hardened concrete. *Constr. Build. Mater.* **2018**, *185*, 661–669. [[CrossRef](#)]
40. Miller, C.D. Kinetics and Mechanism of Alkyl Photooxidation. *Ind. Eng. Chem.* **1958**, *50*, 125–128. [[CrossRef](#)]
41. Fan, L.; Fan, M.; Alhaj, A.; Chen, G.; Ma, H. Hyperspectral imaging features for mortar classification and compressive strength assessment. *Constr. Build. Mater.* **2020**, *251*, 118935. [[CrossRef](#)]

**Disclaimer/Publisher's Note:** The statements, opinions and data contained in all publications are solely those of the individual author(s) and contributor(s) and not of MDPI and/or the editor(s). MDPI and/or the editor(s) disclaim responsibility for any injury to people or property resulting from any ideas, methods, instructions or products referred to in the content.